International Journal of Nanomedicine

Dovepress
open access to scientific and medical research

Open Access Full Text Article

ORIGINAL RESEARCH

Mitigation of Sepsis-Induced Acute Lung Injury by BMSC-Derived Exosomal miR-125b-5p Through STAT3-Mediated Suppression of Macrophage Pyroptosis

Yiming Tao[1,2], Xinxin Xu[1,2], Bin Yang[1,2], Hui Zhao[1,2], Yongsheng Li[1,2]

[1]Department of Critical Care Medicine, Tongji Hospital, Tongji Medical College, Huazhong University of Science and Technology, Wuhan, People's Republic of China; [2]Emergency Department, Tongji Hospital, Tongji Medical College, Huazhong University of Science and Technology, Wuhan, People's Republic of China

Correspondence: Yongsheng Li, Department of Critical Care Medicine, Tongji Hospital, Tongji Medical College, Huazhong University of Science and Technology, 1095 Jiefang Avenue, Qiaokou District, Wuhan, 430030, People's Republic of China, Email tjh_ysli@163.com

Introduction: Sepsis is a syndrome characterized by high morbidity and mortality rates. One of its most severe complications is acute lung injury, which exhibits a multitude of clinical and biological features, including macrophage pyroptosis. This study investigates the regulatory effects of exosomes derived from Bone Marrow-Derived Mesenchymal Stem Cells (BMSCs) on sepsis-associated acute lung injury (ALI) and explores the potential mechanisms mediated by exosomal miRNAs.

Methods: Exosomes were isolated from primary BMSCs of adult C57BL/6J mice using differential centrifugation. Their uptake and distribution in both in vitro and in vivo contexts were validated. Key sepsis-associated hub gene signal transducer and activator of transcription 3 (STAT3) and its upstream non-coding miR-125b-5p were elucidated through a combination of bioinformatics, machine learning, and miRNA sequencing. Subsequently, the therapeutic potential of BMSC-derived exosomes in alleviating sepsis-induced acute lung injury was substantiated. Moreover, the functionalities of miR-125b-5p and STAT3 were corroborated through miR-125b-5p inhibitor and STAT3 agonist interventions, employing gain and loss-of-function strategies both in vitro and in vivo. Finally, a dual-luciferase reporter assay reaffirmed the interaction between miR-125b-5p and STAT3.

Results: We isolated exosomes from primary BMSCs and confirmed their accumulation in the mouse lung as well as their uptake by macrophages in vitro. This study identified the pivotal sepsis-associated hub gene STAT3 and demonstrated that exosomes derived from BMSCs can target STAT3, thereby inhibiting macrophage pyroptosis. MiR-125b-5p inhibition experiments showed that exosomes mitigate macrophage pyroptosis and lung injury by delivering miR-125b-5p. STAT3 overexpression experiments validated that miR-125b-5p reduces macrophage pyroptosis and lung injury by suppressing STAT3. Furthermore, a dual-luciferase reporter assay confirmed the binding interaction between miR-125b-5p and STAT3.

Conclusion: Exosomes derived from BMSCs, serving as carriers for delivering miR-125b-5p, can downregulate STAT3, thereby inhibiting macrophage pyroptosis and alleviating sepsis-associated ALI. These significant findings provide valuable insights into the potential development of ALI therapies centred around exosomes derived from BMSC.

Keywords: mesenchymal stem cells, exosomes, acute lung injury, machine learning, miR-125b-5p, STAT3

Introduction

Sepsis, a condition characterized by inflammation resulting from infections, is responsible for approximately 20% of global deaths each year and exhibits complex pathological and physiological features.[1] Among its complications, acute lung injury (ALI) emerges as an early and severe complication of sepsis, with sepsis serving as a primary etiological factor for ALI.[2] ALI is a life-threatening pathological condition characterized by uncontrolled inflammation leading to damage of the pulmonary endothelial and epithelial cell barriers. The development of sepsis-induced ALI involves

Received: 19 September 2023
Accepted: 21 November 2023
Published: 29 November 2023

complex interactions among various factors, such as pathogens, host immune responses, multi-organ dysfunction, and medical interventions.[3,4] Consequently, patients afflicted by ALI exhibit diverse physiological and biochemical profiles, making it challenging to implement precise therapeutic strategies.[5]

Central to the pathogenesis of ALI are macrophages.[6] Operating within distinct microenvironments during various pathological stages,[7] macrophages contribute to ALI by releasing an array of molecules, undergoing polarization, and experiencing different forms of cell death,[8] all while orchestrating inflammatory cascades.[9] Of particular note, macrophage pyroptosis emerges as a critical factor in ALI.[10] Pyroptosis, a caspase-1-dependent subtype of pro-inflammatory cell death, has a dual role: defending against microbial pathogens and triggering inflammation.[11] However, this inflammation can potentially lead to septic shock.[12] In the context of sepsis-related ALI, macrophage pyroptosis has garnered attention due to its role in releasing inflammatory components that exacerbate inflammation, induce cytokine release, amplify lung inflammation, and damage alveolar membranes. Furthermore, pyroptotic macrophages may lose their immune regulatory functions, disrupting immune homeostasis.[13] Previous studies have demonstrated that lipopolysaccharide (LPS) has the ability to induce alveolar macrophage pyroptosis, thereby worsening lung injury.[14] Targeting alveolar macrophage pyroptosis may offer a promising and innovative therapeutic strategy for managing ALI/ARDS.

Mesenchymal stem cells (MSCs), with their multilineage differentiation potential and anti-inflammatory properties, have shown promise in treating ARDS. They release paracrine factors and extracellular vesicles that exert anti-inflammatory, anti-apoptotic, and antimicrobial effects, while also promoting bacterial and alveolar fluid clearance to prevent lung and distal organ damage.[15] However, the use of MSCs for therapy presents challenges in terms of production and storage, along with an increased risk of immune reactions.[16] In contrast, mesenchymal stem cell-derived exosomes (MSC-Exos) have gained significant attention due to their smaller size, ability to deliver diverse bioactive molecules, and lower immunogenicity.[17] Exosomes are diverse collections of membranous structures secreted by cells, containing a variety of cellular constituents, including microRNAs (miRNAs). MiRNAs, small non-coding RNAs consisting of 21–23 nucleotides, exert post-transcriptional negative control over gene expression by binding to the 3' untranslated region (UTR) of mRNA.[18] These miRNAs play pivotal roles in numerous physiological and biological processes, including cell proliferation, differentiation, organogenesis, and apoptosis regulation. In the context of acute respiratory distress syndrome (ARDS), there is substantial evidence to suggest that the therapeutic effects of MSC-Exos are mediated through the delivery of miRNAs, which can specifically target and regulate host genes.[19]

Utilizing bioinformatics and machine learning methodologies, we have successfully identified STAT3 as a central hub gene,[20] closely associated with cell pyroptosis and sepsis. Furthermore, employing target gene prediction and miRNA sequencing techniques, we have identified miR-125b-5p as a potential binding partner for STAT3. To comprehensively investigate the roles of miR-125b-5p and STAT3 in sepsis-related acute lung injury, we have utilized both in vivo and in vitro models. In vivo, we induced sepsis in mice using lipopolysaccharide (LPS), while in vitro, we employed J774A. 1 cells. Employing functional gain and loss approaches, we aim to elucidate the interaction between miR-125b-5p and STAT3 and its impact on alveolar macrophage pyroptosis and the development of sepsis-related acute lung injury.

The findings of this study suggest that exosomal miR-125b-5p derived from BMSCs may play a critical role in regulating sepsis-induced acute lung injury by suppressing macrophage pyroptosis.

Methods

Cell Culture

We obtained the murine monocyte macrophage cell line, J774A.1, from Procell Life Science & Technology Co., Ltd (China). Cells were cultured in a 5% CO2 humidified environment using DMEM/F12 culture medium supplemented with 10% heat-inactivated fetal bovine serum (FBS) and 1% penicillin/streptomycin in 25 cm2 Cell Culture Flasks (T25). The culture medium was refreshed every 48–72 hours, and cells were subcultured at a 1:3–4 ratio.

Pyroptosis Model

To induce pyroptosis in J774A. 1 cells, we employed a two-step process involving LPS and adenosine triphosphate (ATP). Initially, cells were stimulated with varying concentrations of LPS for 12 hours, followed by the addition of 5 mM ATP for an additional 4 hours to induce macrophage pyroptosis. We determined the optimal LPS concentration using the cell counting kit-

8 (CCK-8) and confirmed pyroptosis through transmission electron microscopy (TEM). Furthermore, J774A. 1 cells were co-cultured with different amounts of exosomes after LPS treatment to assess the optimal exosome dosage, as determined by CCK-8. For the EXO-treated+colivelin group, cells were pre-stimulated with 10 nM colivelin (MedChemExpress, China) for 2 hours before the addition of LPS. Subsequently, the culture medium was replaced to establish the pyroptosis model.

CCK-8 Assay

Cell viability was evaluated by employing the CCK-8 assay (Vazyme, Nanjing, China). J774A.1 cells were seeded in a 96-well plate for 24 hours. After modeling the above steps, add another 10 μL CCK-8 reagent per well and incubated for 2 hours. Absorbance at 450 nm was measured using a microplate reader, and calculations were performed accordingly.

Preparation of BMSCs

Male C57BL/6J mice aged 2–3 weeks were euthanized using cervical dislocation. Following disinfection with 75% alcohol, the femurs and tibias were isolated. The bone marrow cavity was flushed, and the resulting precipitate was collected through centrifugation. Cells obtained from two mice were then seeded in a T25 flask and cultured in MEMα medium (MEMα- riboside/Alanyl-L-glutamine, Pricella, China) supplemented with 10% FBS (HyClone, Canada, US) at 37°C in a humidified atmosphere with 5% CO2. Passages were conducted in a 1:2 ratio until the third generation, after which subsequent passages were determined by cell density.

In order to characterize the cells, we subjected BMSCs to differentiation and culturing processes to generate osteoblasts, adipocytes, and chondrocytes. The multilineage differentiation capacity was assessed through the application of Alizarin Red, Oil Red O, and Alcian Blue staining techniques. Additionally, flow cytometry was utilized to evaluate the surface molecule expression profile of extracted BMSCs (P3-4), specifically targeting CD31, CD44, CD45, and Sca-1, with the use of antibodies sourced from Elabscience (China).

Exosome

Extraction and Identification

BMSCs were cultured until the third generation or beyond. Once the cell confluence reached approximately 60–70% in a complete culture medium, the medium was aspirated, and the cells were rinsed 2–3 times with phosphate-buffered saline (PBS). Subsequently, specialized serum-free culture medium (umibio, China) was introduced, and the cells were cultured for an additional 48 hours until they reached a confluence of 90%. The cell culture supernatant was then collected and subjected to centrifugation at 300g for 10 minutes to remove the cells. The resulting supernatant was subsequently frozen at −80°C. A certain quantity was gathered and subsequently thawed in a consistent manner. Exosomes were obtained using differential centrifugation techniques as described in Figure 1. All centrifugation procedures were performed at a temperature of 4°C.

Exosomes were observed through the utilization of transmission electron microscopy (TEM) with the Hitachi HT-7700 (Japan). 10 ul of exosomes were deposited onto a copper grid and permitted to settle for a duration of one minute. Any surplus liquid was eliminated using filter paper. Subsequently, ten microliters of uranyl acetate were introduced to the grid, and after one minute, any excess liquid was once again removed using filter paper. The grid was then air-dried at ambient temperature for a few minutes prior to imaging at 100 kV.

The homogeneity of exosomes was determined by measuring their size distribution using a particle size analyzer (NanoFCM, N30E). Furthermore, the presence of surface markers including calnexin, TSG101, and CD81 in exosomes was evaluated through Western blotting.

Labeling and Tracking

In vitro

To ascertain the internalization of BMSC-derived exosomes by macrophages, the exosomes were fluorescently labeled with PKH67 dye (umibio, China). Following a 24-hour co-culture of the labeled exosomes with J774a.1 cells in a Confocal Dish, the cells were immobilized. The macrophage cell nuclei were subsequently stained with 4',6-Diamidino-2-phenylindole (DAPI) (Yeasen Biotechnology, China). Ultimately, laser confocal microscopy was employed for imaging.

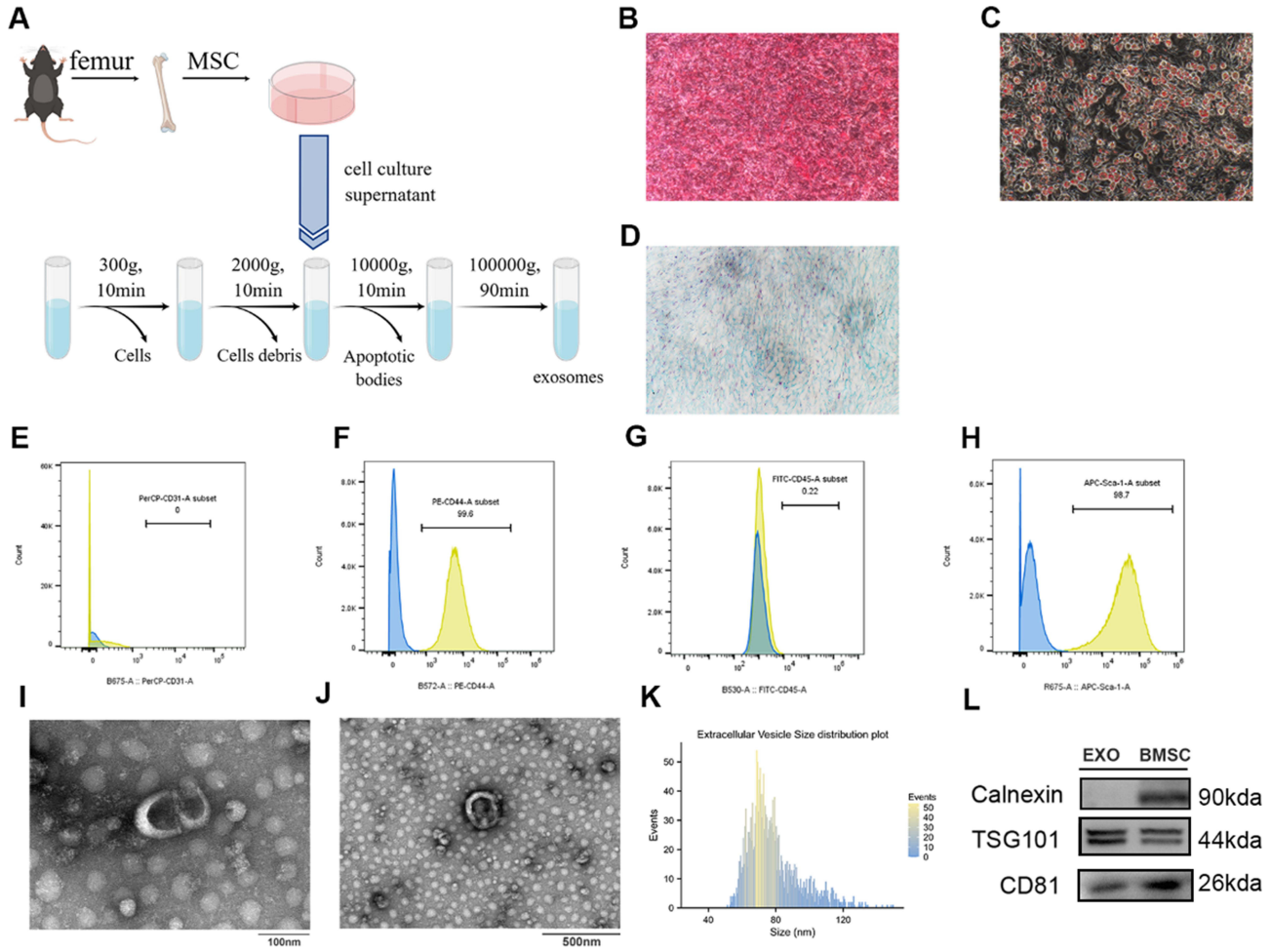

Figure 1 Characterization of BMSCs and exosomes. (**A**) Schematic representation of BMSCs and exosome extraction. (**B**–**D**) Following the induction of osteogenic, chondrogenic, and adipogenic medium, the BMSCs exhibited the presence of alizarin red-positive calcium nodules (**B**), oil-red-O-positive lipid droplets (**C**), a significant amount of acid mucopolysaccharides respectively (**D**) (×200 magnification). The results of flow sorting showed that BMSC expressed high levels of CD44 (**F**) and Sca-1 (**H**), but negative CD31 (**E**) and CD45 (**G**). Morphology of BMSCs exosomes detected by TEM. Scale bar: 100 nm (**I**), 500nm (**J**). (**K**) Diameters distribution of BMSCs exosomes detected by NTA (nm). (**L**) The expression of Calnexin, TSG-101, and CD81 in BMSCs exosomes was detected using Western blot.

In vivo

After inducing sepsis-induced ARDS, mice received tail vein injections of DiR-labeled exosomes (from umibio, China) at different concentrations. Following an 8-hour period and under anesthesia, the mice were subjected to whole-body imaging using an In Vivo Imaging System (IVIS) with an excitation wavelength (λEx) of 748 nm and an emission wavelength (λEm) of 780 nm. Subsequently, the mice were euthanized, and lung tissues were collected for imaging purposes.

Gene Screening

DEGs

We selected the GSE26440 dataset, extracted from the Gene Expression Omnibus (GEO) database, to identify differential expression genes (DEGs). This dataset comprises gene expression data from 98 patients with septic shock and 32 normal controls, with sample collection within the first 24 hours of admission.

To define DEGs, we applied stringent criteria: |Log2Fold-Change| > 0.5 and $P < 0.05$. Subsequently, we conducted Gene Ontology (GO) enrichment analysis and Kyoto Encyclopedia of Genes and Genomes (KEGG) pathway enrichment analysis[21,22] to elucidate the molecular functions and key pathways associated with these DEGs.

Here are detailed insights into the GSE26440 dataset: it includes gene expression data from 98 patients with septic shock and 32 normal controls. Patient samples were collected from whole blood within the first 24 hours of admission.

Comprehensive information about the subjects, including characteristics such as age, illness severity, and mortality rates, is present in this dataset. Controls were incorporated to ensure accurate data normalization.

The original study employed genome-wide expression profiling, utilizing a discovery-oriented expression filter and statistical methods for subclass discovery. To enhance the specificity of subclass identification, leave-one-out cross-validation procedures were employed. This unique experimental design and robust statistical analysis allowed for a thorough exploration of patient subclasses in septic shock, providing clinically relevant insights into patient phenotypes.

We also identified genes related to pyroptosis from the MSigDB database (www.gsea-msigdb.org/gsea/msigdb) and recent publications, followed by an intersection analysis to identify DEGs associated with pyroptosis.

Machine Learning

To enhance the selection of feature genes, we employed statistical learning methods in machine learning on the pyroptosis-associated hub genes. We utilized both Lasso Regression and Random Forest techniques. Lasso Regression, incorporating L1 regularization, was used to promote coefficient sparsity, aiding in identifying features strongly correlated with the target variable and disregarding weaker correlations. The Random Forest algorithm, an ensemble learning method, was employed to rank gene feature importance based on contributions to tree construction and prediction. Thereby aiding in the comprehension of the most crucial genes.

PPI Analysis

Protein-Protein Interaction (PPI) analysis was conducted to validate pivotal genes using the online database STRING (string-db.org) with a confidence level of 0.4.[23] Central genes were identified through degree algorithms and topological analysis facilitated by the CytoHubba plugin in Cytoscape 3.8.0 (University of California, San Diego).

miRNA Sequencing

The composition of exosomes frequently reflects the attributes and conditions of their originating cells, encompassing proteins, RNA, and other molecules. To account for potential variations in exosomes across batches, we performed miRNA sequencing on both BMSCs and J774a. 1 cells to examine differences in miRNA profiles. Sequencing was carried out on the Illumina NovaSeq6000 platform, following the manufacturer's guidelines. Target genes of differentially expressed miRNAs were predicted using the miRDB[24] and TargetScan[25] databases.

Ultimately, the genes identified through machine learning and PPI analysis were cross-referenced with the predicted target genes obtained from the miRDB and TargetScan databases.

Transfection

We introduced miR-125b-5p inhibitor and the corresponding negative control (NC) into BMSCs using InvitroRNA™ (InvivoGene, China) according to the manufacturer's guidelines. BMSCs were cultured in 6-well plates and exposed to the inhibitor or NC in serum-free medium for 24–48 hours. Transfection efficiency was evaluated 1–3 days post-transfection using RT-PCR. Transfected cells were used for subsequent experimental procedures.

Histopathological Assessment of Lung Tissue

To assess the extent of lung injury, lung tissues were obtained 72 hours post-modeling, fixed in 4% paraformaldehyde, and paraffin-embedded. Sections (4μm) were stained with hematoxylin and eosin (H&E). Lung injury severity was assessed using a previously literature described lung injury scoring system[26] (The lung injury scoring criteria are provided in the Supplementary Table 1).

Measurement of Pulmonary Vascular Permeability

Pulmonary vascular permeability was evaluated by measuring the pulmonary wet-to-dry weight ratio (W/D). The trachea and esophagus were dissected using a blunt technique, and the samples were then weighed to determine their wet weight. Subsequently, the samples underwent a drying process at a temperature of 60°C for a duration of 60 hours until they reached a state of complete dryness, and the dry weight was subsequently measured.

Western Blotting

Protein extraction from lung tissue and cells was performed using RIPA Lysis Buffer supplemented with a protease and phosphatase inhibitor cocktail (MedChemExpress, China). For cell culture supernatant protein extraction, an equal volume of methanol was added to the supernatant, followed by vortexing. Subsequently, chloroform (200 μL) was added, and after centrifugation, the upper methanol layer was discarded. Fresh methanol was added, followed by centrifugation. The resulting pellet was then treated with ethanol, vortexed, and centrifuged to collect the protein pellet.

The concentration of proteins was determined using the Bicinchoninic Acid (BCA) protein assay kit (Abbkine, China). Approximately 30μg of protein extracts were separated by 10% sodium dodecyl sulfate-polyacrylamide gel electrophoresis (SDS-PAGE) and transferred onto PVDF membrane (Bio-Rad, Shanghai). Subsequently, the membrane was blocked with 5% skim milk (Servicebio) at room temperature for 2 hours and incubated overnight at 4°C with specific primary antibodies (Antibody information is provided in Supplementary Table 2). The next day, the membrane was probed with corresponding secondary antibodies and detected using the Super ECL reagent (MedChemExpress). The target protein was normalized to β-actin, and quantification was performed using ImageJ software (NIH).

Measurement of Inflammatory Cytokines

The collection and centrifugation of bronchoalveolar lavage fluid (BALF) from mice that underwent successful modeling at a speed of 980 rpm for a duration of 15 minutes resulted in the collection of the supernatant. Furthermore, the supernatant from cell cultures after modeling was also collected. Both samples were utilized for the quantification of tumor necrosis factor-alpha (TNF-α), interleukin-6 (IL-6), and interleukin-18 (IL-18) levels using ELISA assay kits (ABclonal, China).

Flow Cytometry

As previously mentioned, the cell precipitate obtained from the centrifuged BALF of mice was used for flow cytometry analysis. Fc receptors were blocked using CD16/32 (BD Pharmingen) to minimize non-specific staining during the staining procedure. Lung alveolar macrophages were identified using CD45 and Anti-F4/80 antibody (BD Pharmingen). Alveolar macrophage pyroptosis levels were quantified using 7-Aminoactinomycin D (BD Pharmingen) and caspase-1 (USbiological). Flow cytometry experiments were conducted using a six-color high-throughput flow cytometer (Neon-1026M, Sanci), and data were analyzed using FlowJo software.

RT-qPCR

Total RNA was extracted from J774a.1 and BMSCs using TRIzol reagent (TaKaRa Bio, Japan). Following the removal of genomic DNA, cDNA was synthesized using a stem-loop primer for mmu-miR-125b-5p (Vazyme, China) and an RT primer for other mRNAs. Subsequently, qPCR was conducted using the SYBR Green Premix Pro Taq HS qPCR kit (Accurate biotechnology, China). U6 and β-actin were employed as internal reference controls for miRNA and mRNA, respectively. The primer sequences utilized in this study can be found in Supplementary Table 3.

Dual-Luciferase Reporter Assay

STAT3-WT/MT gene sequences were constructed and cloned into the pmirGLO vector, which contains both Firefly luciferase and Renilla luciferase. Synthetic mimics of miR-125b-5p and NC were prepared. The pmirGLO empty vector, wild-type or mutant STAT3, and miR-125b-5p mimics/NC were co-transfected into 293T cells. After 48 hours, luciferase activity was measured using the Dual-Luciferase Reporter Gene Assay System (Promega). (The Supplementary Table 4 displays the precise sequences of STAT3-WT/MT and the mimics/NC of miR-125b-5p).

The Animal Models

Male C57BL/6J mice, aged 6–8 weeks, were obtained from Beijing Vital River Laboratory Animal Technology Co. Ltd. A portion of the younger mice were bred in-house by mating male and female mice of appropriate age. All animals were housed in our specialized animal facilities, ensuring specific pathogen-free conditions. The Institutional Animal Care and Use Committee of the Academic Medical Center granted ethical approval and oversight for our study. The control group of mice received a 50 μL

intratracheal injection of PBS as a control treatment. In the treatment groups, 2 hours after intratracheal LPS injection, a tail vein injection of $2*10^9$ exosomes, with or without a miR-125b-5p inhibitor, was administered. In the STAT3 agonist Colivelin group (MedChemExpress, China), a peritoneal injection of Colivelin (1 mg/kg) was performed within 2 hours after intratracheal LPS injection, in addition to the tail vein injection of exosomes. Subsequent Colivein injections were administered at 24-hour intervals, totaling three injections. The remaining groups were administered 200 μL of PBS injections. Following the establishment of the model, mice were euthanized after an initial 72-hour period in order to prepare for subsequent experiments.

Statistical Analysis

The R software (version 4.3.0) was utilized for conducting bioinformatics analysis and machine learning. In cases where the data satisfied the assumptions of normal distribution and homogeneity of variances, a *t*-test was employed for comparing two groups, while a one-way analysis of variance (ANOVA) was utilized for comparing three groups. In cases where the data adhered to a normal distribution but did not meet the assumption of homogeneity of variances, Welch's one-way ANOVA was utilized. When the data did not conform to a normal distribution, the Wilcoxon test was utilized for two-group comparisons, and the Kruskal–Wallis test was employed for comparisons among three or more groups. All data are expressed as mean ± standard deviation (SD).

Result

Extraction and Identification

BMSCs

BMSCs were extracted using the method outlined in Figure 1A. The BMSCs isolated from murine bone marrow exhibited a spindle-like morphology. When exposed to osteogenic, chondrogenic, and adipogenic differentiation media, the BMSCs displayed specific features, such as the presence of alizarin red-positive calcium nodules (Figure 1B), oil red O-positive lipid droplets (Figure 1C), and an abundance of alcian blue-positive acidic glycosaminoglycans (Figure 1D). The identity of BMSCs was further confirmed through flow cytometry analysis, which revealed elevated expression levels of CD44 and Sca-1, while CD31 and CD45 exhibited negative expression (Figure 1E–H). These findings serve as evidence supporting the assertion that the isolated cells are BMSCs.

BMSC-Derived Exosomes

Initially, the morphology of exosomes was examined using TEM. The observed particles exhibited a rounded or oval shape, possessed a bilayer membrane structure, and had an approximate diameter of 100 nm (Figure 1I and J). Subsequent analysis of the particles was conducted using a particle size analyzer (NanoFCM, N30E), which revealed a particle concentration of $4.3*10^{10}$ Particles/mL. The majority of the particles fell within the size range of 50–120 nm, with a median diameter of 74.25nm and an average diameter of 78.40nm (Figure 1K). Finally, Western blot analysis of exosome-specific markers revealed low expression of Calnexin and high expression of TSG101 and CD81 (Figure 1L). Based on these comprehensive findings, the particles derived from our BMSC isolation were unequivocally identified as exosomes.

Model Establishment

The J774a.1 cells were subjected to stimulation with different concentrations of LPS for a duration of 12 hours. This was followed by a 4-hour treatment with 5mM ATP to establish the cell pyroptosis model. The assessment of cell viability through CCK-8 assays demonstrated a significant reduction in cell viability when the LPS concentration reached 500 ng/mL, as compared to the group with lower LPS concentrations ($p<0.05$) (Figure 2A). Upon re-establishing the model using this protocol, TEM observations revealed that the majority of macrophages exhibited pyroptotic features, characterized by cell swelling, disruption of cell membrane integrity, reduced and degraded pseudopods (PS), and the release of certain contents into the extracellular space. The cells displayed moderate cytoplasmic swelling, nearly round cell nuclei (N) with slight nuclear condensation, moderate mitochondrial swelling, and degradation of ridge structures (Figure 2B, indicated by thick arrows). The rough endoplasmic reticulum (RER) exhibited notable expansion (Figure 2B, indicated by thick arrows).[25] Approximately $2*10^5$ J774a.1 cells were seeded in each well of a 6-well plate, and exosomes were added at a concentration of $1*10^2$–$2*10^2$ particles/cell, followed by the induction of pyroptosis under the conditions described earlier. CCK-8 results demonstrated that both quantities of exosomes significantly improved the cell viability of macrophages under the pyroptosis model. The mean cell viability was higher when

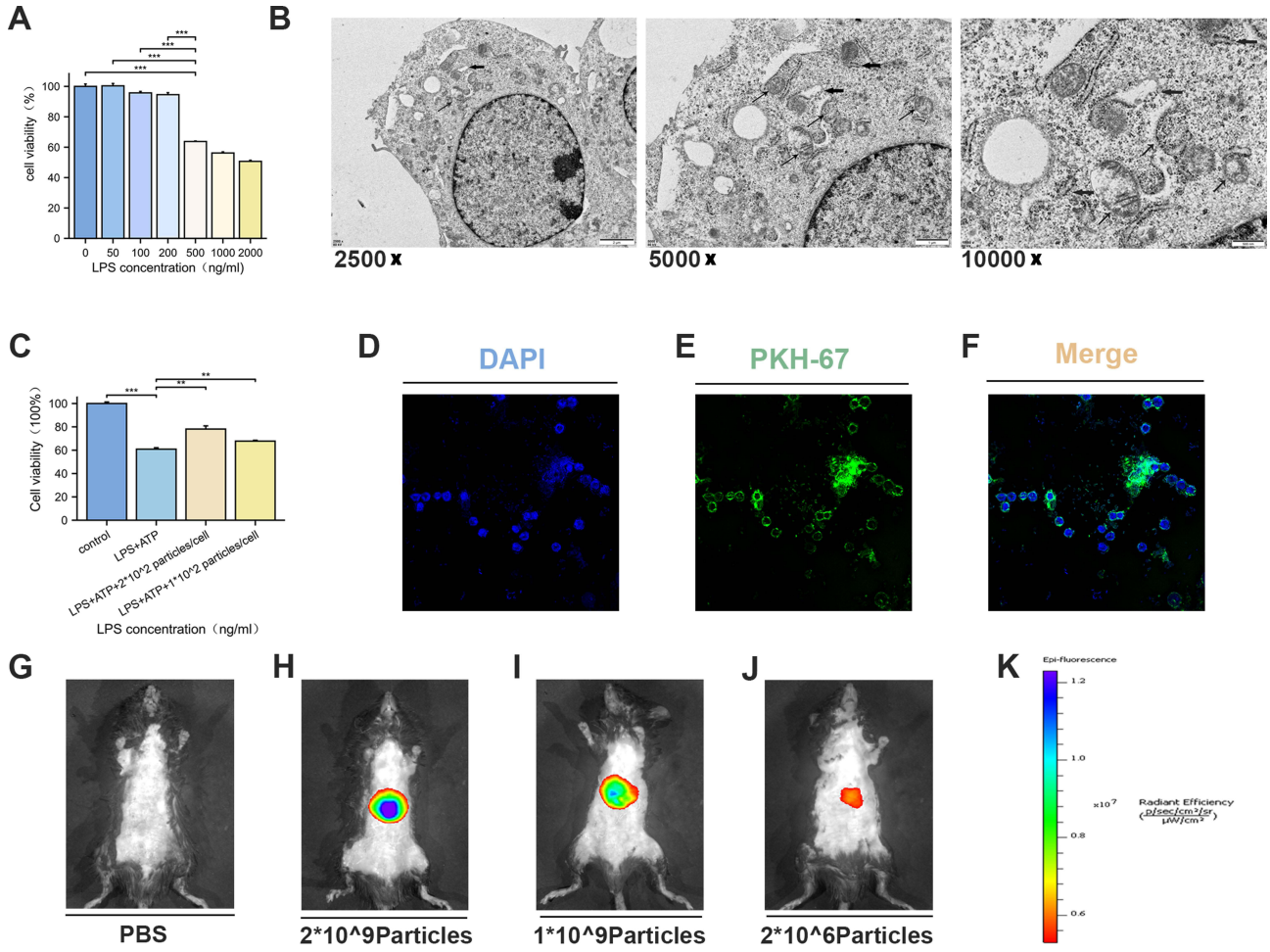

Figure 2 Model establishment and exosome labeling and tracking. (**A**) Determination of optimal LPS concentrations for J774a.1 cells using the Cell Counting Kit-8. (**B**) TEM images of J774a.1 cells (left: ×2500 magnification; middle: ×5000 magnification; right: ×10,000 magnification). (**C**) Assessment of various concentrations of exosome effects on J774a.1 cells using the Cell Counting Kit-8. (**D**–**F**) Internalization of BMSCs exosomes by J774a.1 cells, visualized with blue (DAPI) and green (PKH67 labeled BMSCs exosomes) fluorescence. (**G**–**K**) Distribution of different amounts of BMSCs exosomes in mice: PBS (**G**), 2×10^9 particles (**H**), 1×10^9 particles (**I**), 2×10^6 particles (**J**), and a fluorescence intensity table (**K**). (Control: control group; LPS+ATP: pyroptosis modeling group; LPS+ATP+$2*10^2$ particles/cell and LPS+ATP+$1*10^2$ particles/cell refer to the groups treated with different quantities of exosomes following pyroptosis modeling.) Each experiment was repeated at least three times, and the data are presented as mean ± SEM (**P<0.01, ***P<0.001).

using a concentration of $2*10^2$ particles/cell compared to $1*10^2$ particles/cell, although this difference did not reach statistical significance (Figure 2C). Nonetheless, the model was established utilizing the $2*10^2$ particles/cell regimen in order to optimize the therapeutic effect.

Labeling and Tracking

In vitro

In order to ascertain the internalization of exosomes derived from BMSCs by J774a.1 cells, the exosomes were subjected to labeling with PKH-67 (green) and subsequently co-cultured with macrophages. The utilization of confocal microscopy demonstrated the successful internalization of the labeled exosomes by the macrophages, as depicted in Figure 2D–F.

In vivo

After administering tail vein injections of DiR-labeled exosomes at varying concentrations and PBS, fluorescence imaging analysis revealed the absence of detectable signals in mice injected with PBS. Conversely, mice injected with exosomes exhibited prominent signals in the chest region, with the highest intensity observed in those injected with $2*10^9$ particles (Figure 2G–K). Subsequent lung fluorescence imaging confirmed a substantial accumulation of exosomes in the lungs (Figure S1A). Consequently, a treatment dosage of $2*10^9$ particles per mouse was chosen for subsequent experimental procedures.

Gene Selection

Through bioinformatics analysis, a total of 2427 DEGs were identified from the GSE26440 dataset, comprising 1368 upregulated and 1059 downregulated genes (Figure 3A). Enrichment analysis of the differentially expressed genes revealed enrichment in processes related to immune response regulation and macrophage activation in GO molecular function analysis (Figure 3B). KEGG pathway enrichment analysis indicated pathways associated with cell death mechanisms such as Autophagy, Ferroptosis, and Apoptosis (Figure 3C). The intersection of DEGs and genes related to pyroptosis revealed 15 co-expressed genes (Figure 3D).

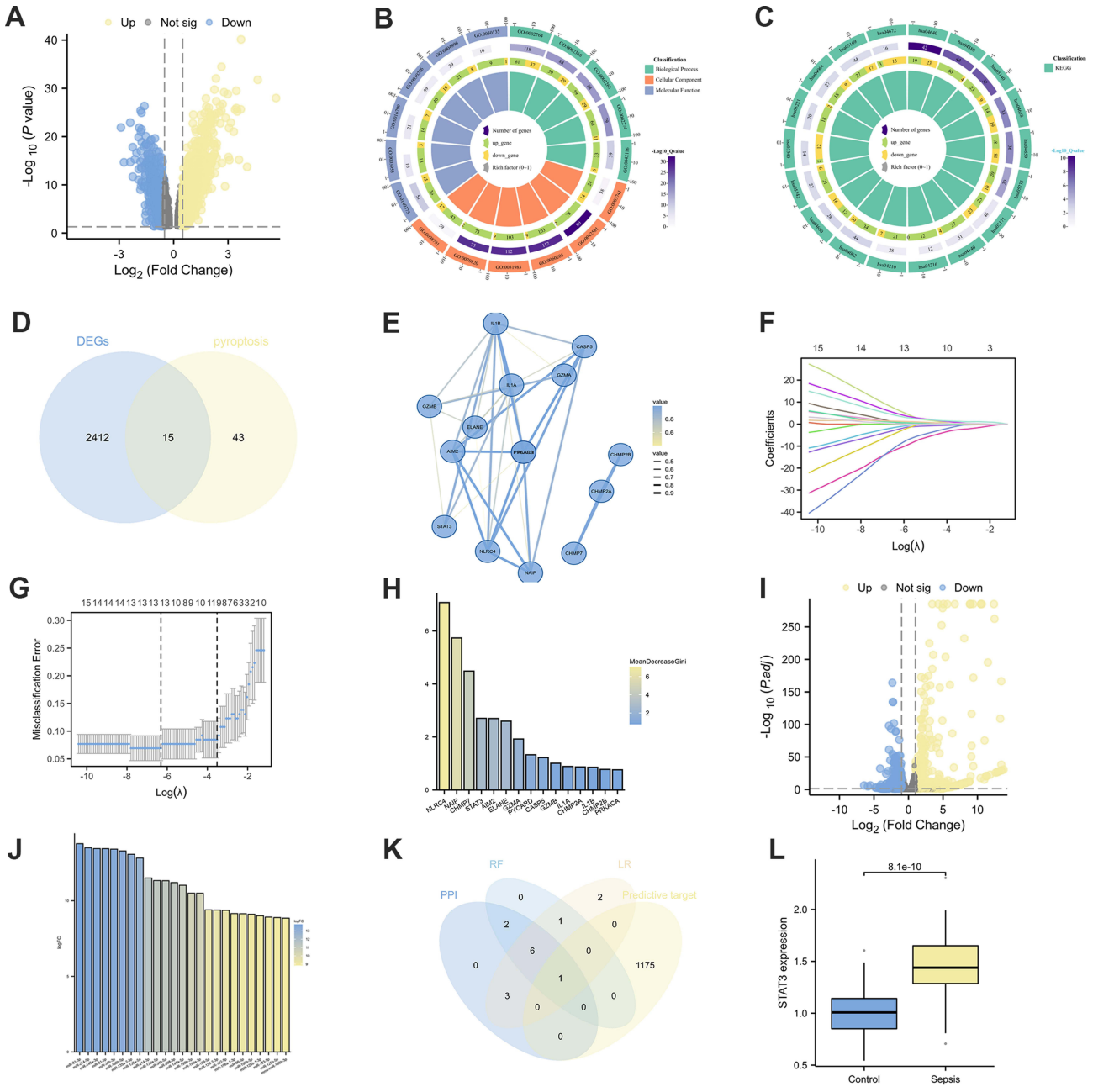

Figure 3 Gene Selection. (**A**) The volcano plot shows the DEGs in GSE26440. (**B**) GO enrichment analysis of DEGs. (**C**) KEGG enrichment analysis of DEGs. (**D**) A Venn diagram program was used to reflect the intersection between DEGs and pyroptosis-related genes. (**E**) PPI network of intersected genes. (**F**–**G**) lasso regression analysis of intersected genes: Coefficient Plot (**F**), Parameter Plot (**G**). (**H**) Random forest analysis of intersected genes. (**I**) Volcano plot regarding differentially expressed miRNAs between BMSC and J774a.1. (**J**) In the highly expressed miRNAs among BMSCs, the top 25 miRNAs with the highest gene expression levels. (**K**) A Venn diagram was used to represent the intersections between multiple machine learning screening genes and predicted target genes of miRNAs. (**L**) STAT3 expression in healthy people and sepsis patients in GSE26440 dataset.

PPI network analysis using Cytoscape software identified 12 central genes (Figure 3E). The Lasso regression method identified 13 feature genes (Figure 3F and G), and random forest ranked all 15 genes based on their feature importance scores (meandecreasegini) (Figure 3H). Subsequently, differential analysis of miRNA sequencing data identified 532 differentially expressed genes. Among them, 287 were upregulated, and 245 were downregulated in BMSCs (Figure 3I). The top 25 miRNAs with the highest expression levels in BMSCs were selected (Figure 3J). The 25 miRNAs with high expression levels were utilized for target gene prediction through the utilization of miRDB and TargetScan databases (Figure S1B and C), resulting in the identification of 1176 target genes. Subsequently, a Venn diagram analysis was conducted to examine the central genes derived from the PPI analysis, the feature genes identified by Lasso regression, the top 10 genes determined by their importance in random forest, and the predicted target genes (Figure 3K). Ultimately, the central gene STAT3 and its interacting target gene miR-125b-5p were successfully identified. Validation in the GSE26440 dataset confirmed a significant increase in STAT3 RNA expression levels in sepsis patients ($p<0.05$) (Figure 3L).

Mitigation of Sepsis-Induced ARDS by Alleviating Macrophage Pyroptosis with BMSC-Derived Exosomes

To elucidate the therapeutic potential of BMSC-derived exosomes, a multifaceted approach was employed to assess macrophage pyroptosis levels and the severity of ARDS in control, sepsis-induced ARDS, and exosome-treated groups. The lung W/D weight ratio results revealed significantly increased pulmonary vascular permeability in the sepsis-induced mouse model compared to the control group, while exosome treatment notably attenuated pulmonary vascular permeability (Figure 4A). ELISA analysis of cell culture supernatant demonstrated consistent trends in inflammatory markers such as IL-6, TNF-α, and IL-18, which are associated with both inflammation and pyroptosis severity, aligning with the W/D ratio findings. The changes of IL-6, IL-18 displayed statistical significance (Figure 4B–D). BALF supernatant ELISA results from mice were in substantial agreement with the cell culture supernatant data (Figure 4E–G).

Flow cytometry, following the isolation of lung alveolar macrophages by CD45 and F4/80 markers, confirmed a significantly elevated pyroptosis rate in the ARDS model compared to the control group, whereas BMSC-derived exosomes prominently alleviated lung alveolar macrophage pyroptosis (Figure 4H and I). Evaluation of ARDS severity using the lung injury scoring system indicated that LPS inflicted severe lung tissue damage, while BMSC-derived exosomes demonstrated a mitigating effect on lung tissue injury (Figure 4J, K; Figure S2A–C).

Furthermore, Western blot analysis revealed increased expression of pyroptosis-related proteins and p-STAT3 following pyroptosis induction. However, treatment with BMSC-derived exosomes reversed the increasing trend in protein expression (Figure 4L–U). Specifically, in vivo experiments showed significant upregulation of NLRP3, p-STAT3, GSDMD-N, caspase-1, cleaved caspase-1, and IL-1β in the sepsis-induced group, which was attenuated by exosome treatment. Except that the expression of caspase-1 did not change significantly, the results of in vitro experiment were in good concordance with in vivo results (Figure S2D–K).

In conclusion, this study demonstrates that BMSC-derived exosomes alleviate sepsis-induced ARDS by mitigating macrophage pyroptosis.

Alleviation of Sepsis-Induced ARDS by BMSC-Derived Exosomes via miR-125b-5p Modulation

To elucidate the role of miR-125b-5p in sepsis-induced ARDS, exosomes secreted by miR-125b-5p inhibitor-transfected BMSCs were administered to J774a.1 cells and mice. The results of the lung W/D weight ratio analysis indicated that inhibition of miR-125b-5p expression attenuated the exosome-mediated reduction in pulmonary vascular permeability (Figure 5A). Furthermore, ELISA results from both in vivo and in vitro experiments demonstrated that the groups treated with anti-miR-125b-5p exosomes exhibited reduced anti-inflammatory and anti-pyroptotic capabilities compared to the groups treated with exosomes alone. Specifically, in vitro experiments showed significant reductions in IL-6 and IL-18 (Figure 5B–D), and in vivo experiments demonstrated statistical significance in IL-6 and TNF-α (Figure 5E–G). Moreover, flow cytometry and pathological scoring revealed that exosomes with inhibited miR-125b-5p expression

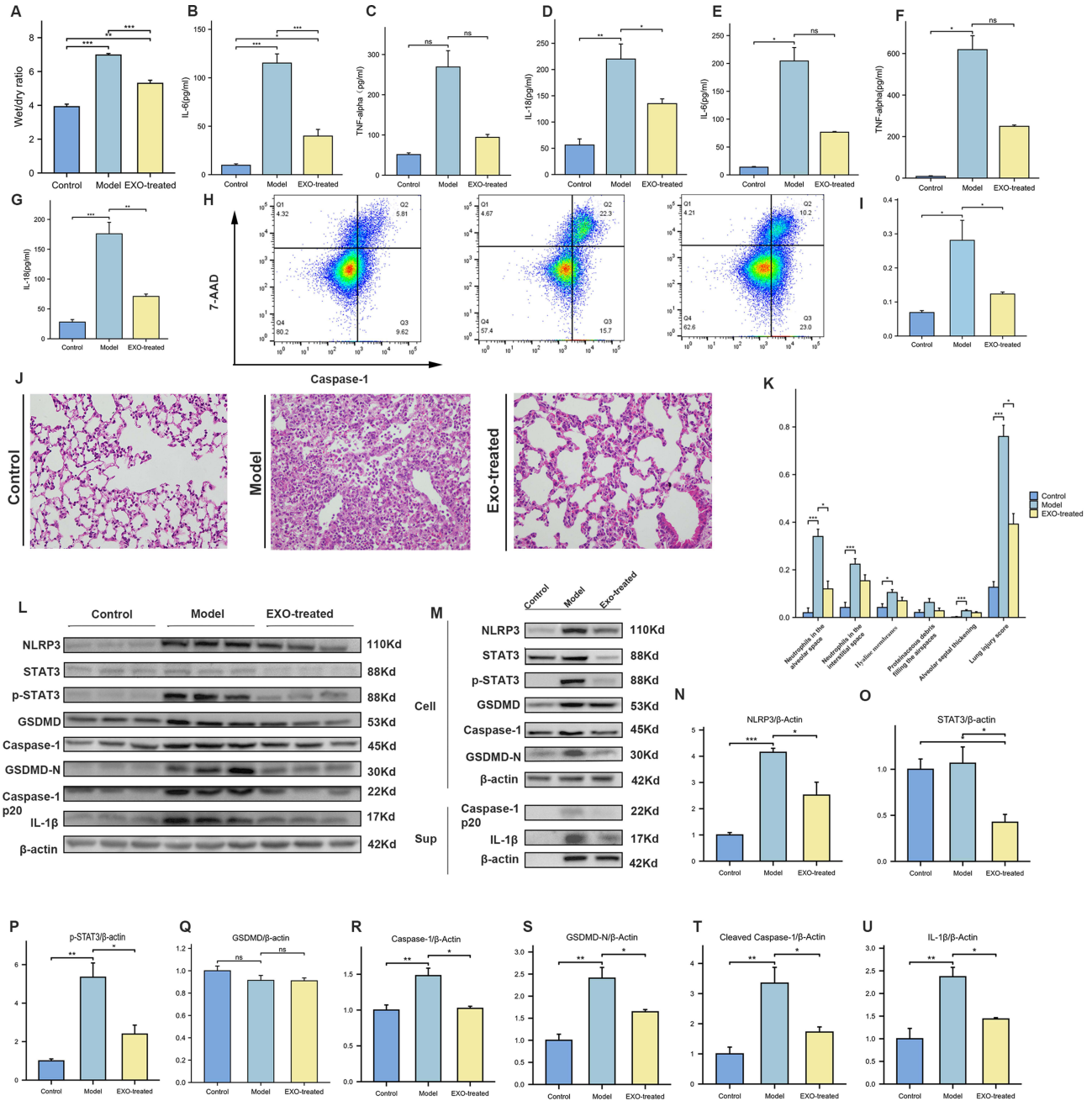

Figure 4 Mitigation of Sepsis-Induced ARDS by Alleviating Macrophage Pyroptosis with BMSC-Derived Exosomes. (**A**) The lung W/D ratio was assessed to evaluate lung edema. (**B**–**D**) The levels of inflammatory and pyroptosis-related factors in the cell supernatant were assessed via ELISA:IL-6 (**B**), TNF-α (**C**), IL-18 (**D**). (**E**–**G**) The levels of inflammatory and pyroptosis-related factors in the BALF were assessed via ELISA:IL-6 (**E**), TNF-α (**F**), IL-18 (**G**). (**H**) Flow cytometry analysis of Caspase-1/7-AAD staining and quantification of the Pyroptotic macrophages. (**I**) Flow cytometric analysis of the percentage of pyroptosis macrophages. (**J**) Histopathological images of lung tissue (×400 magnification). (**K**) lung injury score based on pathological images of lung tissue. (**L**) NLRP3, STAT3, P-STAT3, GSDMD, Caspase-1,GSDMD-N, cleaved caspase-1, IL-1β and β-actin expressions of differently treated mice were detected by Western blot. (**M**) Western blot was performed to assess protein expression in J774a.1 cells following different treatments (Cell represents proteins extracted from within the cells, Sup represents proteins extracted from the cell supernatant). (**N**–**U**) Bar charts quantify the relative expression levels of various proteins in lung tissue. (Control, control group; Model, pyroptosis modeling group; EXO-treated, treated with exosomes following pyroptosis modeling.) Every experiment was repeated at least three times, and the data was shown as mean ± SEM (ns: no difference,*P<0.05,**P<0.01, ***P<0.001).

exhibited reduced effectiveness in mitigating lung alveolar macrophage pyroptosis (Figure 5H and I) and ameliorating lung tissue structural damage caused by ARDS (Figure 5J, K; Figure S3A–D) compared to exosomes without miR-125b-5p inhibition. Furthermore, Western blot analysis conducted on lung tissues indicated a reduced capacity to inhibit the expression of NLRP3, p-STAT3, cleaved caspase-1, and IL-1β in the inhibition group when compared to the group

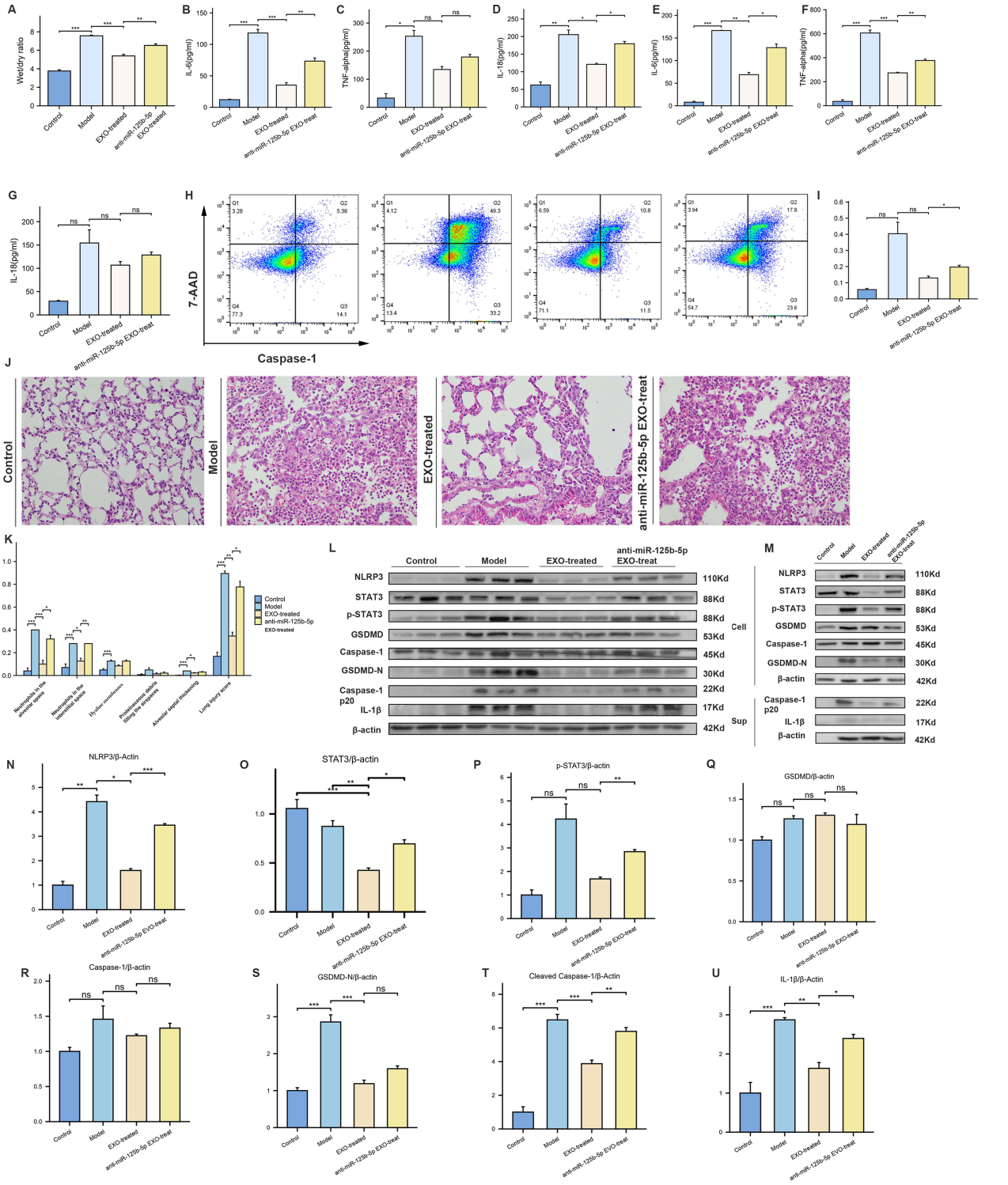

Figure 5 Alleviation of Sepsis-Induced ARDS by BMSC-Derived Exosomes via miR-125b-5p Modulation. (**A**) The lung W/D ratio was assessed to evaluate lung edema. (**B**–**D**) The levels of inflammatory and pyroptosis-related factors in the cell supernatant were assessed via ELISA:IL-6 (**B**), TNF-α (**C**), IL-18 (**D**). (**E**–**G**) The levels of inflammatory and pyroptosis-related factors in the BALF were assessed via ELISA:IL-6 (**E**), TNF-α (**F**), IL-18 (**G**). (**H**) Flow cytometry analysis of Caspase-1/7-AAD staining and quantification of the pyroptosis macrophages. (**I**) Flow cytometric analysis of the percentage of pyroptotic macrophages. (**J**) Histopathological images of lung tissue (×400 magnification). (**K**) lung injury score based on pathological images of lung tissue. (**L**) NLRP3, STAT3, P-STAT3, GSDMD, Caspase-1, GSDMD-N, cleaved caspase-1, IL-1β and β-actin expressions of differently treated mice were detected by Western blot. (**M**) Western blot was performed to assess protein expression in J774a.1 cells following different treatments (Cell represents proteins extracted from within the cells, Sup represents proteins extracted from the cell supernatant). (**N**–**U**) Bar charts quantify the relative expression levels of various proteins in lung tissue. (Control, control group; Model, pyroptosis modeling group; EXO-treated, treated with exosomes following pyroptosis modeling; anti-miR-125b-5p EXO-treat, following the establishment of the pyroptosis model, treatment was administered using exosomes derived from BMSCs transfected with inhibitor of miR-125b-5p.) Every experiment was repeated at least three times, and the data was shown as mean ± SEM (ns: no difference,*P<0.05,**P<0.01, ***P<0.001).

treated with exosomes (Figure 5L–U). The findings from in vitro experiments demonstrated that the group treated with anti-miR-125b-5p EXO-treat group exhibited a capacity to suppress the expression of STAT3, p-STAT3, and pyroptosis-associated proteins. However, this inhibitory effect was comparatively weaker than that observed in the EXO-treated group. Furthermore, the expression pattern observed in the in vitro experiments was largely consistent with the outcomes of the in vivo experiment (Figure S3E–L). These results provide evidence that miR-125b-5p present in BMSC-Exo mitigates macrophage pyroptosis and the development of sepsis-induced ARDS.

BMSC-Derived Exosomes Alleviate Sepsis-Induced ARDS by Modulating STAT3

The previously mentioned findings provide evidence that LPS triggers macrophage pyroptosis and lung tissue damage in mice, while exosomes derived from BMSCs alleviate LPS-induced macrophage pyroptosis, ameliorate lung tissue injury, and reduce the expression of STAT3 and p-STAT3. In order to further confirm the involvement of STAT3 and p-STAT3 in macrophage pyroptosis and ARDS, we utilized the STAT3 activator colivelin.

The lung W/D weight ratio results showed that the pulmonary vascular permeability in the EXO-treat+Colivelin group was higher than that in the EXO-treat group, although this difference was statistically insignificant (Figure 6A). Furthermore, the results obtained from ELISA experiments demonstrated a notable reduction in the anti-inflammatory and anti-pyroptotic capabilities of exosome therapy following STAT3 activation, both in vitro and in vivo. In vitro cell experiments showed a marked increase in IL-6 and TNF-α levels in the EXO-treat+Colivelin group compared to the EXO-treat group (Figure 6B–D), while in vivo experiments demonstrated significant elevations in IL-6, TNF-α, and IL-18, all with statistical significance (Figure 6E–G).

The flow cytometry results for levels of lung alveolar macrophage pyroptosis are presented in Figure 6H and I, indicating a notable increase in pyroptosis following activation of STAT3. Additionally, the pathological scoring demonstrates that STAT3 activation results in more severe lung tissue damage, as shown in (Figure 6J, K; Figure S4A–D). Moreover, Western blotting analysis of lung tissues, as depicted in Figure 6L–U, reveals significant elevations in pyroptosis-related proteins, including NLRP3, cleaved caspase-1, and IL-1β, in the EXO-treat+Colivelin group compared to the EXO-treat group. While the combined treatment of exosomes and Colivelin partially suppressed STAT3 expression, it resulted in a noticeable increase in p-STAT3 expression compared to the group treated solely with exosomes. The expression pattern observed in the in vitro experiments was largely consistent with the outcomes of the in vivo experiment (Figure S4E–L). In conclusion, these findings suggest that exosomes derived from BMSCs mitigate macrophage pyroptosis and ARDS induced by sepsis through the downregulation of STAT3 and p-STAT3 expression.

Regulation of STAT3 by BMSC-Derived Exosomes via miR-125b-5p

Relative Expression Levels of miR-125b-5p and STAT3

We transfected BMSCs with miR-125b-5p inhibitor and miR-NC and then extracted RNA from both J774a.1 and BMSCs. We subsequently conducted RT-qPCR to assess the expression levels of miR-125b-5p. As shown in Figure 7A, the expression levels of miR-125b-5p in non-transfected BMSCs and BMSCs transfected with miR-NC were significantly higher than in BMSCs transfected with the miR-125b-5p inhibitor, with no significant difference observed between the former two groups. In contrast, J774a.1 cells exhibited much lower levels of miR-125b-5p expression across all groups. Furthermore, following the induction of pyroptosis, the expression levels of miR-125b-5p in J774a.1 cells decreased further. Irrespective of the transfection of the miR-125b-5p inhibitor, BMSC-derived exosomes demonstrated a substantial capacity to transfer miR-125b-5p into J774a.1 cells. Nevertheless, the transfection of the miR-125b-5p inhibitor resulted in a discernible decrease in this transfer capability (Figure 7B). Furthermore, the utilization of RT-qPCR analysis on J774a.1 cells subjected to various treatment groups demonstrated a noteworthy elevation in STAT3 mRNA levels within macrophages following pyroptosis induced by LPS and ATP. Subsequent treatment with exosomes derived from BMSCs resulted in a conspicuous reduction in the relative expression levels of STAT3. However, the suppressive impact on STAT3 expression exerted by exosomes was significantly diminished upon transfection of the miR-125b-5p inhibitor (Figure 7C). These results collectively indicate that the intracellular levels of miR-125b-5p in BMSCs are substantially higher than those in J774a.1 cells. Moreover, BMSC-derived exosomes effectively transmit miR-125b-5p into J774a.1 cells, resulting in the downregulation of STAT3 mRNA expression.

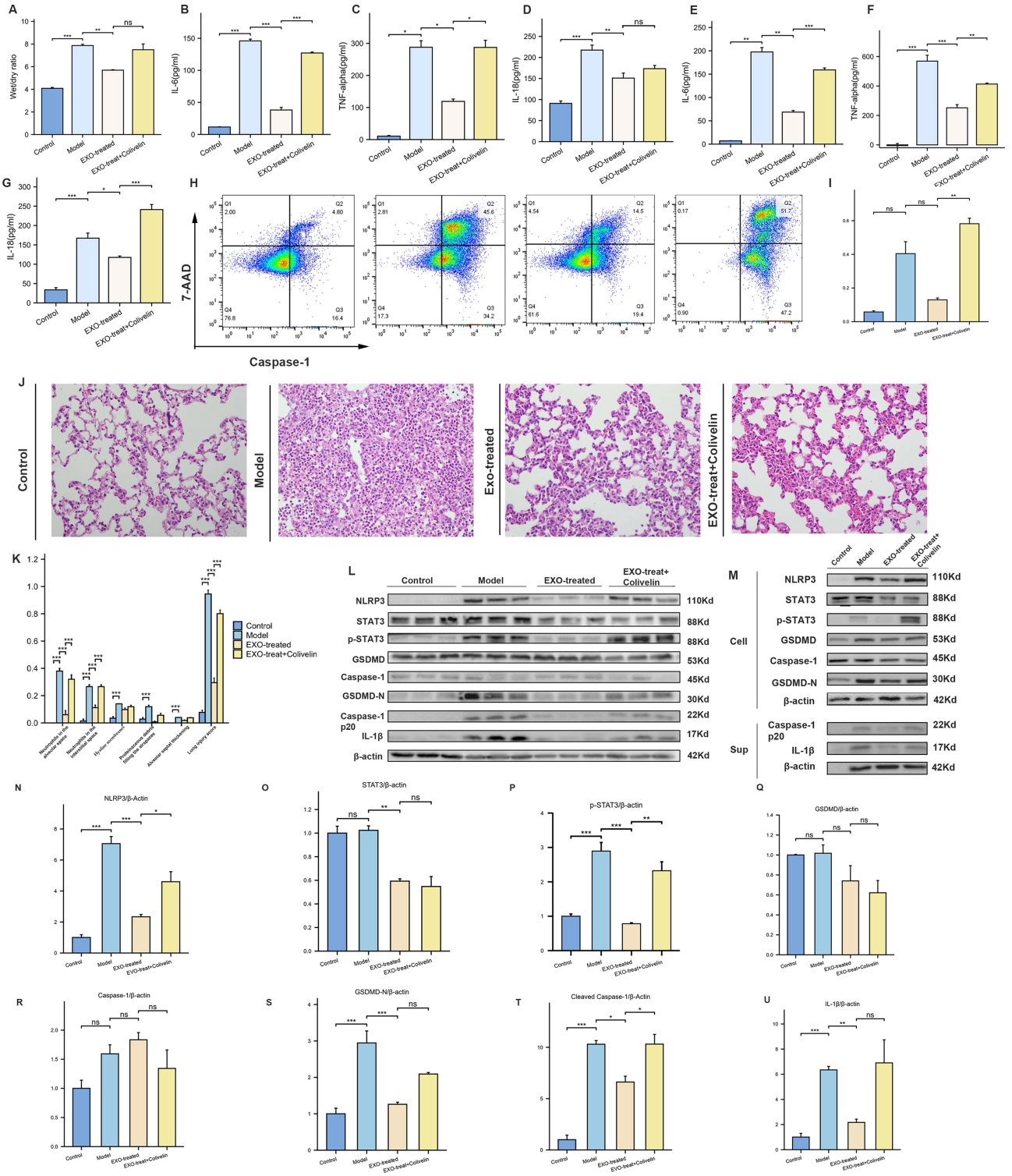

Figure 6 BMSC-Derived Exosomes Alleviate Sepsis-Induced ARDS by Modulating STAT3. (**A**) The lung W/D ratio was assessed to evaluate lung edema. (**B**–**D**) The levels of inflammatory and pyroptosis-related factors in the cell supernatant were assessed via ELISA:IL-6 (**B**), TNF-α (**C**), IL-18 (**D**). (**E**–**G**) The levels of inflammatory and pyroptosis-related factors in the BALF were assessed via ELISA:IL-6 (**E**), TNF-α (**F**), IL-18 (**G**). (**H**) Flow cytometry analysis of Caspase-1/7-AAD staining and quantification of the pyroptosis macrophages. (**I**) Flow cytometric analysis of the percentage of pyroptotic macrophages. (**J**) Histopathological images of lung tissue (×400 magnification). (**K**) lung injury score based on pathological images of lung tissue. (**L**) NLRP3, STAT3, P-STAT3, GSDMD, Caspase-1, GSDMD-N, cleaved caspase-1, IL-1β and β-actin expressions of differently treated mice were detected by Western blot. (**M**) Western blot was performed to assess protein expression in J774a.1 cells following different treatments (Cell represents proteins extracted from within the cells, Sup represents proteins extracted from the cell supernatant). (**N**–**U**) Bar charts quantify the relative expression levels of various proteins in lung tissue. (Control, control group; Model, pyroptosis modeling group; EXO-treated, treated with exosomes following pyroptosis modeling; EXO-treat+Colivelin, The group undergoing pyroptosis modeling concurrently with the administration of colivelin.) Every experiment was repeated at least three times, and the data was shown as mean ± SEM (ns: no difference, P≥0.05,*P<0.05,**P<0.01, ***P<0.001).

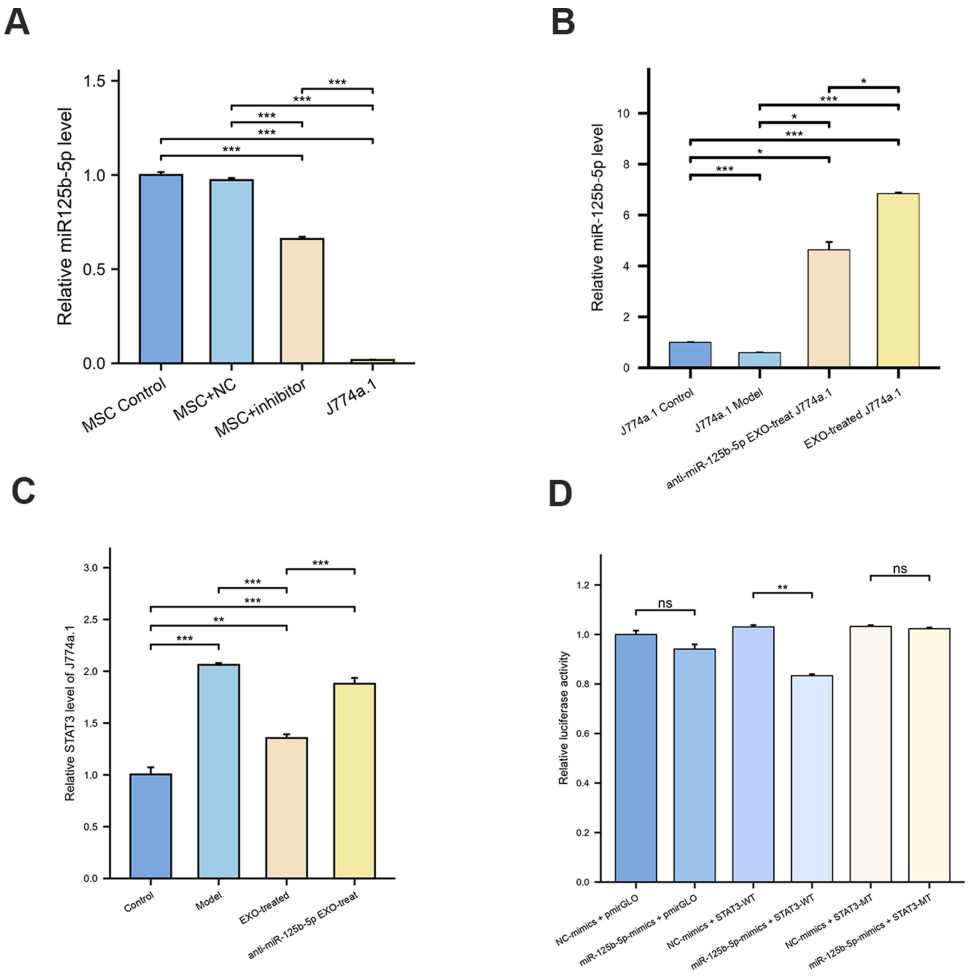

Figure 7 (**A**) PCR results showed the relative expression of miR-125b-5p in different treatment groups. (**B**) Relative expression of miR-125b-5p in J774a.1 cells of different treatment groups. (**C**) PCR results showed the relative expression of STAT3 in J774a.1 cells of different treatment groups. (**D**) The targeted modulation measured by luciferase reporter gene assays. Every experiment was repeated at least three times, and the data was shown as mean ± SEM (ns: no difference,*P<0.05,**P<0.01, ***P<0.001).

Dual-Luciferase Reporter Assay

MiRNAs exert their functions through interaction with the 3'UTR or protein coding sequences of target mRNAs.[26] To establish the direct association between miR-125b-5p and its target gene STAT3, we employed a Dual-luciferase reporter assay to validate the interaction between miR-125b-5p and STAT3. This assay involved the use of renilla luciferase as an internal control, and the relative light units (RLU) obtained from firefly luciferase measurements were divided by the RLU obtained from renilla luciferase measurements. Comparing the resulting ratio between different samples allowed us to assess the activity level of the target reporter gene. In the comparison between the miR-125b-5p-mimics + pmirGLO empty vector group and the NC-mimics + pmirGLO empty vector group, no statistically significant alteration in fluorescence values was observed. Conversely, when comparing the miR-125b-5p-mimics + STAT3-WT group with the NC-mimics + STAT3-WT group, a significant reduction in fluorescence values was noted. Similarly, in the comparison between the miR-125b-5p-mimics + STAT3-MT group and the NC-mimics + STAT3-MT group, no significant change in fluorescence values was observed. These results suggest that STAT3 might be a downstream target of miR-125b-5p (Figure 7D).

Discussion

This study aimed to investigate the potential therapeutic efficacy of exosomes derived from BMSCs in the treatment of ARDS. Our findings revealed that BMSC-derived exosomes exhibited the ability to accumulate within the lungs of mice

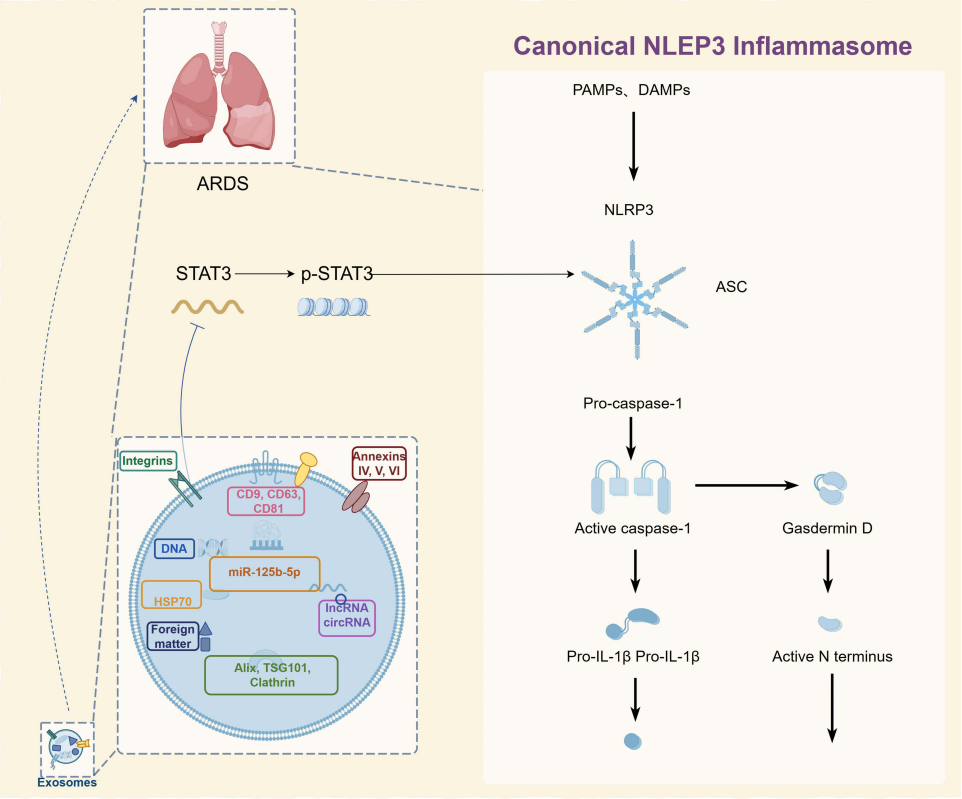

Figure 8 Schematic diagram of the extracted BMSC exosomal miR-125b-5p inhibiting pyroptosis and thereby alleviating ARDS by negatively regulating STAT3.

in vivo and were internalized by macrophages in vitro. Importantly, we demonstrated for the first time that BMSC-derived exosomes can attenuate macrophage pyroptosis via the miR-125b-5p/STAT3 pathway, thereby mitigating the progression of ARDS (Figure 8).

Sepsis, a syndrome characterized by life-threatening dysfunction of organs,[27] often presents with acute lung injury, which is an early and highly fatal complication.[28] Alveolar macrophages, being the primary immune cells in the alveoli, play a vital role in the development of sepsis-induced ARDS.[7] These macrophages contribute to the maintenance of lung homeostasis by phagocytosing bacteria, eliminating cellular debris, and regulating inflammatory proteins.[29] However, when infections get out of control, alveolar macrophages may lose their balance, manifesting polarization and various forms of cell death, which continuously promote inflammation,[8] thereby leading to the progression of ARDS.[30] Among these forms, pyroptosis, which relies on the activation of caspase-1, represents a unique type of cellular demise.[11] Pyroptosis is distinguished by cellular enlargement, swift rupture of the plasma membrane, and the discharge of pro-inflammatory substances, thereby intensifying the inflammatory reaction.[31] There is substantial evidence indicating that macrophage pyroptosis enhances inflammation during ARDS and exacerbates lung inflammation,[32,33] and inhibiting alveolar macrophage pyroptosis can reduce lipopolysaccharide-induced acute lung injury in mice.[34] Therefore, targeting alveolar macrophage pyroptosis is a rational strategy for treating ARDS. MSCs are cells with pluripotency, immunomodulation, and differentiation functions that have been widely used for treating various human diseases by regulating immune responses, reducing inflammation, primarily through their paracrine pathways.[35] Among their paracrine products, exosomes are the main secretory substances of BMSCs.[36] MSCs exist in various tissues such as bone marrow, adipose tissue, and umbilical cord, but research on BMSCs is the most extensive so far.[37] Therefore, we chose BMSCs as the source of exosomes to explore their potential role in ARDS treatment.

We initially observed that when administered via the tail vein, MSC-exos exhibited a preferential tropism for injured lungs. Typically, MSC-exos tend to accumulate primarily in the livers and spleens of mice, followed by the lungs and kidneys.[38,39] However, in sepsis-induced ARDS mice, with a significant accumulation of exosomes in the thoracic and

abdominal regions, especially in the lungs. This indicates that MSC-exos may represent a promising therapeutic and drug delivery strategy for ARDS. Subsequently, after confirming the therapeutic effect of BMSC exosomes on lung by vascular permeability, pathological score and other methods, We further explored STAT3, a key gene associated with pyroptosis in sepsis-induced ARDS, and miR-125b-5p, which is highly expressed in MSC-exos and binds to STAT3 to play a therapeutic role by inhibiting macrophage pyroptosis.

MiR-125b-5p belongs to the miR-125 family, which is a highly conserved microRNA found in various species from nematodes to humans.[40] It participates in cell differentiation, proliferation, and apoptosis by targeting messenger RNAs associated with these processes and is implicated in various diseases such as cancer, cardiovascular diseases, and autoimmune conditions.[41,42] In the context of ARDS, miR-125b-5p has been found to fulfill various significant functions. Shen et al conducted a study indicating that miR-125b-5p, present in adipose-derived stem cell exosomes, can ameliorate acute lung injury in sepsis by regulating the expression of STAT3.[43] Additionally, Peng et al demonstrated that miR-125b-5p exhibits anti-inflammatory properties in AMs during sepsis, thereby mitigating septic lung injury.[44] In the present study, it was observed that the inhibition of miR-125b-5p resulted in a reduction of the protective effect exerted by MSC-exos and their ability to inhibit macrophage pyroptosis in mice with ARDS. This finding provides the first confirmation that miR-125b-5p ameliorates ARDS through the inhibition of macrophage pyroptosis. Nevertheless, it is important to note that this does not negate the potential protective effects of other miRNAs present in BMSC exosomes or other targets regulated by miR-125b-5p, as previously mentioned.

Further investigation was conducted on the protective mechanism of the miR-125b-5p/STAT3 pathway in ARDS. STAT3 is a pivotal signaling protein that plays a crucial role in the regulation of immune and inflammatory responses. Activation of STAT3 occurs through phosphorylation (p-STAT3) by receptor tyrosine kinases (RTKs) and various cytokines. p-STAT3 exhibits enhanced nuclear translocation and DNA binding ability, thereby effectively modulating the expression of downstream genes. STAT3 plays a significant role in the regulation of numerous diseases by modulating various cellular processes, such as cell proliferation, differentiation, autophagy, and apoptosis.[45,46] Notably, recent research has increasingly focused on the influence of STAT3 on the progression of different diseases through the regulation of cell death, including sepsis and lung injury.[47,48] Additionally, certain studies have demonstrated that p-STAT3 facilitates the acetylation of histone H3 and H4 on the NLRP3 promoter, as well as the activation of the NLRP3 inflammasome, which may be directly regulated by p-STAT3.[48] Furthermore, several studies have demonstrated the impact of STAT3 on pyroptosis through its influence on other targets, including AIM2 and GSDME.[49,50] Consequently, the modulation of STAT3 presents a promising therapeutic approach for mitigating sepsis-induced ARDS by suppressing macrophage pyroptosis.

In conclusion, our study has provided insights into a novel therapeutic mechanism involving the delivery of miR-125b-5p through BMSC-derived exosomes to mitigate macrophage pyroptosis by modulating STAT3 expression, leading to the amelioration of sepsis-induced acute lung injury. This discovery presents a promising strategy for the future treatment of sepsis-related ARDS. However, it is important to note that our investigation primarily focused on the therapeutic effects of miR-125b-5p within BMSC exosomes, specifically targeting STAT3 mRNA and subsequently influencing the protein expression of STAT3 and p-STAT3. It's important to note that the expression of STAT3 is also subject to post-transcriptional regulation, post-translational modifications, and other processes. Whether miR-125b-5p or other miRNAs within BMSCs play a role in these physiological processes remains to be further explored. Furthermore, the molecular mechanisms underlying the interaction between STAT3 and other pyroptotic pathways as well as other forms of cell death are also worthy of further investigation.

Conclusion

In summary, this study sheds light on the significant role of miR-125b-5p and unveils a novel mechanism involving BMSC-derived exosomes in the treatment of sepsis and sepsis-related ARDS. These findings open new avenues for innovative ARDS therapies and hold promise for improving patient outcomes. However, it is essential to underscore that the clinical efficacy and safety of BMSC-derived exosomes warrant further rigorous in vivo investigations. Additionally, the intricate molecular mechanisms underlying these therapeutic effects remain the focus of ongoing research.

Consequently, the clinical translation of BMSCs, including their exosomes, necessitates continued comprehensive exploration.

Ethics Approval and Consent to Participate

Animal experimental procedures of this study were approved by the Animal Ethics Committee at Tongji Hospital (TJH-202206038). The Laboratory Animal Guidelines for Ethical Review of Animal Welfare (GB/T 35892-2018) was followed to ensure the welfare of the laboratory animals.

Funding

This study was financially supported by the Beijing medical and health foundation (YWJKJJHKYJJ—BXS5—22001).

Disclosure

The authors report no conflicts of interest in this work.

References

1. Rudd KE, Johnson SC, Agesa KM, et al. Global, regional, and national sepsis incidence and mortality, 1990–2017: analysis for the Global Burden of Disease Study. *Lancet*. 2020;395(10219):200–211. doi:10.1016/S0140-6736(19)32989-7
2. Martin GS, Mannino DM, Eaton S, Moss M. The epidemiology of sepsis in the United States from 1979 through 2000. *N Engl J Med*. 2003;348(16):1546–1554. doi:10.1056/NEJMoa022139
3. Schuurman AR, Sloot PMA, Wiersinga WJ, van der Poll T. Embracing complexity in sepsis. *Crit Care*. 2023;27(1):102. doi:10.1186/s13054-023-04374-0
4. Singer M. Sepsis: personalization v protocolization? *Crit Care*. 2019;23(S1):127. doi:10.1186/s13054-019-2398-5
5. Sinha P, Meyer NJ, Calfee CS. Biological phenotyping in sepsis and acute respiratory distress syndrome. *Annu Rev Med*. 2023;74(1):457–471. doi:10.1146/annurev-med-043021-014005
6. Vichare R, Janjic JM. Macrophage-targeted nanomedicines for ARDS/ALI: promise and potential. *Inflammation*. 2022;45(6):2124–2141. doi:10.1007/s10753-022-01692-3
7. Tao H, Xu Y, Zhang S. The role of macrophages and alveolar epithelial cells in the development of ARDS. *Inflammation*. 2023;46(1):47–55. doi:10.1007/s10753-022-01726-w
8. Chen X, Tang J, Shuai W, Meng J, Feng J, Han Z. Macrophage polarization and its role in the pathogenesis of acute lung injury/acute respiratory distress syndrome. *Inflamm Res*. 2020;69(9):883–895. doi:10.1007/s00011-020-01378-2
9. Khalaj K, Figueira RL, Antounians L, Lauriti G, Zani A. Systematic review of extracellular vesicle-based treatments for lung injury: are EVs a potential therapy for COVID-19? *J Extracell Vesicles*. 2020;9(1):1795365. doi:10.1080/20013078.2020.1795365
10. Li N, Liu B, He R, et al. HDAC3 promotes macrophage pyroptosis via regulating histone deacetylation in acute lung injury. *iScience*. 2023;26(7):107158. doi:10.1016/j.isci.2023.107158
11. Wei X, Xie F, Zhou X, et al. Role of pyroptosis in inflammation and cancer. *Cell Mol Immunol*. 2022;19(9):971–992. doi:10.1038/s41423-022-00905-x
12. Chen R, Zeng L, Zhu S, et al. cAMP metabolism controls caspase-11 inflammasome activation and pyroptosis in sepsis. *Sci Adv*. 2019;5(5):eaav5562. doi:10.1126/sciadv.aav5562
13. Chan FKM, Luz NF, Moriwaki K. Programmed necrosis in the cross talk of cell death and inflammation. *Annu Rev Immunol*. 2015;33(1):79–106. doi:10.1146/annurev-immunol-032414-112248
14. Jiao Y, Zhang T, Zhang C, et al. Exosomal miR-30d-5p of neutrophils induces M1 macrophage polarization and primes macrophage pyroptosis in sepsis-related acute lung injury. *Crit Care*. 2021;25(1):356. doi:10.1186/s13054-021-03775-3
15. Qin H, Zhao A. Mesenchymal stem cell therapy for acute respiratory distress syndrome: from basic to clinics. *Protein Cell*. 2020;11(10):707–722. doi:10.1007/s13238-020-00738-2
16. Doron G, Temenoff JS. Culture substrates for improved manufacture of mesenchymal stromal cell therapies. *Adv Healthcare Mater*. 2021;10(15):2100016. doi:10.1002/adhm.202100016
17. Shah TG, Predescu D, Predescu S. Mesenchymal stem cells-derived extracellular vesicles in acute respiratory distress syndrome: a review of current literature and potential future treatment options. *Clin Transl Med*. 2019;8(1). doi:10.1186/s40169-019-0242-9
18. Shang R, Lee S, Senavirathne G, Lai EC. microRNAs in action: biogenesis, function and regulation. *Nat Rev Genet*. 2023;24(12):816–833. doi:10.1038/s41576-023-00611-y
19. Xiong C, Huang X, Chen S, Li Y, Siddiqui A. Role of extracellular microRNAs in sepsis-induced acute lung injury. *J Immunol Res*. 2023;2023:5509652. doi:10.1155/2023/5509652
20. Fleuren LM, Klausch TLT, Zwager CL, et al. Machine learning for the prediction of sepsis: a systematic review and meta-analysis of diagnostic test accuracy. *Intensive Care Med*. 2020;46(3):383–400. doi:10.1007/s00134-019-05872-y
21. Carbon S, Douglass E, Good BM, et al.; The Gene Ontology Consortium. The Gene Ontology resource: enriching a GOld mine. *Nucleic Acids Res*. 2021;49(D1):D325–D334. doi:10.1093/nar/gkaa1113
22. Yu G, Wang LG, Han Y, He QY. clusterProfiler: an R package for comparing biological themes among gene clusters. *OMICS*. 2012;16(5):284–287. doi:10.1089/omi.2011.0118
23. Szklarczyk D, Gable AL, Lyon D, Junge A, Wyder S. STRING v11: protein-protein association networks with increased coverage, supporting functional discovery in genome-wide experimental datasets. *Nucleic Acids Res*. 2019;47(D1):607–613. doi:10.1093/nar/gky1131

24. Betel D, Wilson M, Gabow A, et al. The microRNA.org resource: targets and expression. *Nucleic Acids Res*. 2008;36:D149–D153. doi:10.1093/nar/gkm995
25. Lewis BP, Shih IH, Jones RM, et al. Prediction of mammalian microRNA targets. *Cell*. 2003;115(7):787–798. doi:10.1016/s0092-8674(03)01018-3
26. Kulkarni HS, Lee JS. Update on the Features and Measurements of Experimental Acute Lung Injury in Animals: An Official American Thoracic Society Workshop Report. *Am J Respir Cell Mol Biol*. 2022;66(2):e1–e14. doi:10.1165/rcmb.2021-0531ST
27. Vandewalle J, Libert C. Sepsis: a failing starvation response. *Trends Endocrinol Metab*. 2022;33(4):292–304. doi:10.1016/j.tem.2022.01.006
28. Maddali MV, Churpek M, Pham T, et al. Validation and utility of ARDS subphenotypes identified by machine-learning models using clinical data: an observational, multicohort, retrospective analysis. *Lancet Respir Med*. 2022;10(4):367–377. doi:10.1016/S2213-2600(21)00461-6
29. Su Y, Silva JD, Doherty D, et al. Mesenchymal stromal cells-derived extracellular vesicles reprogramme macrophages in ARDS models through the miR-181a-5p-PTEN-pSTAT5-SOCS1 axis. *Thorax*. 2023;78(6):617–630. doi:10.1136/thoraxjnl-2021-218194
30. Zheng Y, Huang Y, Xu Y, Sang L, Liu X, Li Y. Ferroptosis, pyroptosis and necroptosis in acute respiratory distress syndrome. *Cell Death Discov*. 2023;9(1):91. doi:10.1038/s41420-023-01369-2
31. Yu P, Zhang X, Liu N, Tang L, Peng C, Chen X. Pyroptosis: mechanisms and diseases. *Signal Transduct Target Ther*. 2021;6(1):128. doi:10.1038/s41392-021-00507-5
32. Xia X, Wang X, Zheng Y, Jiang J, Hu J. What role does pyroptosis play in microbial infection? *J Cell Physiol*. 2019;234(6):7885–7892. doi:10.1002/jcp.27909
33. Liu B, Li Y, Xiang J, et al. Significance of pyroptosis in immunoregulation and prognosis of patients with acute respiratory distress syndrome: evidence from RNA-Seq of alveolar macrophages. *J Inflamm Res*. 2023;16:3547–3562. doi:10.2147/JIR.S422585
34. Wu DD, Pan PH, Liu B, et al. Inhibition of alveolar macrophage pyroptosis reduces lipopolysaccharide-induced acute lung injury in mice. *Chin Med J*. 2015;128(19):2638–2645. doi:10.4103/0366-6999.166039
35. Wang Y, Fang J, Liu B, Shao C, Shi Y. Reciprocal regulation of mesenchymal stem cells and immune responses. *Cell Stem Cell*. 2022;29(11):1515–1530. doi:10.1016/j.stem.2022.10.001
36. Arya SB, Collie SP, Parent CA. The ins-and-outs of exosome biogenesis, secretion, and internalization. *Trends Cell Biol*. 2023. doi:10.1016/j.tcb.2023.06.006
37. Galipeau J, Sensébé L. Mesenchymal stromal cells: clinical challenges and therapeutic opportunities. *Cell Stem Cell*. 2018;22(6):824–833. doi:10.1016/j.stem.2018.05.004
38. Betzer O, Barnoy E, Sadan T, et al. Advances in imaging strategies for in vivo tracking of exosomes. *Wiley Interdiscip Rev Nanomed Nanobiotechnol*. 2020;12(2):e1594. doi:10.1002/wnan.1594
39. Aimaletdinov AM, Gomzikova MO. Tracking of extracellular vesicles' biodistribution: new methods and approaches. *Int J Mol Sci*. 2022;23(19):11312. doi:10.3390/ijms231911312
40. Le MTN, Teh C, Shyh-Chang N, et al. MicroRNA-125b is a novel negative regulator of p53. *Genes Dev*. 2009;23(7):862–876. doi:10.1101/gad.1767609
41. Zhu LP, Tian T, Wang JY, et al. Hypoxia-elicited mesenchymal stem cell-derived exosomes facilitates cardiac repair through miR-125b-mediated prevention of cell death in myocardial infarction. *Theranostics*. 2018;8(22):6163–6177. doi:10.7150/thno.28021
42. Tiedt S, Prestel M, Malik R, et al. RNA-Seq identifies circulating miR-125a-5p, miR-125b-5p, and miR-143-3p as potential biomarkers for acute ischemic stroke. *Circ Res*. 2017;121(8):970–980. doi:10.1161/CIRCRESAHA.117.311572
43. Shen K, Wang X, Wang Y, et al. miR-125b-5p in adipose derived stem cells exosome alleviates pulmonary microvascular endothelial cells ferroptosis via Keap1/Nrf2/GPX4 in sepsis lung injury. *Redox Biol*. 2023;62:102655. doi:10.1016/j.redox.2023.102655
44. Peng W, Yang Y, Chen J, et al. Small extracellular vesicles secreted by iPSC-derived MSCs ameliorate pulmonary inflammation and lung injury induced by sepsis through delivery of miR-125b-5p. *J Immunol Res*. 2023;2023:8987049. doi:10.1155/2023/8987049
45. Zhang YG, Zhu X, Lu R, et al. Intestinal epithelial HMGB1 inhibits bacterial infection via STAT3 regulation of autophagy. *Autophagy*. 2019;15(11):1935–1953. doi:10.1080/15548627.2019.1596485
46. Gong H, Tao Y, Xiao S, et al. LncRNA KIAA0087 suppresses the progression of osteosarcoma by mediating the SOCS1/JAK2/STAT3 signaling pathway. *Exp Mol Med*. 2023;55(4):831–843. doi:10.1038/s12276-023-00972-8
47. Wang X, Guo Z, Wang Z, et al. Diagnostic and predictive values of pyroptosis-related genes in sepsis. *Front Immunol*. 2023;14:1105399. doi:10.3389/fimmu.2023.1105399
48. Liu Y, Yang H, Zhu F, Ouyang Y, Pan P. Inhibition of STAT3 phosphorylation by colchicine regulates NLRP3 activation to alleviate sepsis-induced acute lung injury. *Inflammopharmacol*. 2023;31(4):2007–2021. doi:10.1007/s10787-023-01199-9
49. Zhu SY, Li CX, Tong YX, Xu YR, Wang ZY, Li JL. IL-6/STAT3/Foxo1 axis as a target of lycopene ameliorates the atrazine-induced thymic mitophagy and pyroptosis cross-talk. *Food Funct*. 2022;13(17):8871–8879. doi:10.1039/d2fo01497a
50. Wei Y, Lan B, Zheng T, et al. GSDME-mediated pyroptosis promotes the progression and associated inflammation of atherosclerosis. *Nat Commun*. 2023;14(1):929. doi:10.1038/s41467-023-36614-w